Fluctuation of lysosomal protein degradation in neural stem cells of the postnatal mouse brain

He Zhang[1], Karan Ishii[1,‡], Tatsuya Shibata[1], Shunsuke Ishii[2], Marika Hirao[1], Zhou Lu[1], Risa Takamura[1], Satsuki Kitano[3], Hitoshi Miyachi[3], Ryoichiro Kageyama[4], Eisuke Itakura[2], Taeko Kobayashi[1,*,§]

[1]Graduate School of Biostudies, Kyoto University, Kyoto 606-8315, Japan
[2]Graduate School of Science, Chiba University, Chiba, 263-8555, Japan
[3]Institute for Life and Medical Sciences, Kyoto University, Kyoto 606-8507, Japan
[4]RIKEN Center for Brain Science, Wako, Saitama 351-0198, Japan

[*]Author for correspondence: kobayashi-tk@g.ecc.u-tokyo.ac.jp
[‡]Present address: Department of Cell and Systems Biology, University of Toronto, Toronto, Ontario, M5S 3G5, Canada
[§]Present address: The Institute of Medical Science, The University of Tokyo, Tokyo 108-8639, Japan

Summary statement
Lysosomal proteolytic activity fluctuates in neural stem cells in the dentate gyrus of juvenile, adult, aged, and diseased brains.

Lysosomes are intracellular organelles responsible for degrading diverse macromolecules delivered from several pathways, including the endo-lysosomal and autophagic pathways. Recent reports have suggested that lysosomes are essential for regulating neural stem cells in developing, adult, and aged brains. However, the activity of these lysosomes has yet to be monitored in these brain tissues. Here, we report the development of a new probe to measure lysosomal protein degradation in brain tissue by immunostaining. Our results indicate that lysosomal protein degradation fluctuates in neural stem cells of the hippocampal dentate gyrus, depending on age and brain

disorders. Neural stem cells increase their lysosomal activity during hippocampal development in the dentate gyrus, but aging and aging-related disease reduce lysosomal activity. In addition, physical exercise increases lysosomal activity in neural stem cells and astrocytes in the dentate gyrus. We therefore propose that three different stages of lysosomal activity exist: the state of increase during development, the stable state during adulthood, and the state of reduction due to damage caused by either age or disease.

Introduction

Lysosomes are membrane-bound organelles used to degrade biological macromolecules that also serve as a signal transduction hub after sensing intracellular amino acid levels (Ballabio and Bonifacino, 2020). They also function in lipid metabolism and calcium storage. Recent reports have suggested that lysosomal regulation plays essential roles in neural stem cells (NSCs) in developing, adult, and aged brains (Kobayashi et al., 2019; Leeman et al., 2018; Yuizumi et al., 2021). Neural stem cells are present in two regions of the adult brain: the subventricular zone of the lateral ventricles (SVZ) and the dentate gyrus of the hippocampus (DG) (Fuentealba et al., 2012). In the developmental stage, neural stem/progenitor cells (NSPCs) located in the SVZ contain many more lysosomes than neurons of the developing telencephalon (Yuizumi et al., 2021). Lysosomal deficiency leads to premature differentiation of NSPCs due to reduced expression of the lysosomal transporter for histidine and peptides (Yuizumi et al., 2021).

Slowly dividing NSPCs, which are the likely source of adult NSCs in the SVZ (Furutachi et al., 2015; Urban and Guillemot, 2014), are enriched in lysosomes. Enhanced lysosomal biogenesis induced by ectopic expression of constitutively active mutants of TFEB, a master transcription factor for lysosomal biogenesis, suppresses the cell cycle of NSPCs in the embryonic brain (Yuizumi et al., 2021). NSPCs enter the quiescent state to maintain NSCs for an extended time in the adult brain. Quiescent NSCs in the DG contain enriched lysosomes, and their deficiency reactivates quiescent NSCs after the accumulation of activated EGF and Notch receptors (Kobayashi et al., 2019). Lysosomes in quiescent NSCs in the SVZ store protein aggregates (Leeman et al., 2018), and quiescence exit clears these aggregates to recover their proteostasis for proliferation in the DG (Morrow et al., 2020). Especially in the aged brain, quiescent NSCs in the SVZ accumulate more protein aggregates in their lysosomes, reducing reactivation ability. The enhancement of lysosomal biogenesis reduces the incidence of aggregates and recovers the reactivation from quiescent NSCs in the SVZ (Leeman et al., 2018). These reports all demonstrate that lysosomes are involved in NSC

maintenance in the brain; however, how the protein degradation by lysosomes differs at different stages and conditions in these NSCs *in vivo* has not yet been analyzed in detail. Recently, fluorescent probes have become available for monitoring biological activities, including signal transduction and protein degradation (Mizushima and Murphy, 2020; Neefjes and Dantuma, 2004). Autophagy flux probes have been used in the adult brain to determine that autophagy-lysosome function is impaired in neurons before pathogenesis with lowered v-ATPase activity (Lee et al., 2022).

In this report, we demonstrate a novel lysosomal probe containing two fluorescent proteins with differing stability to monitor lysosomal protein degradation activity in NSCs of the mouse hippocampus from juvenile to old ages (Ishii et al., 2019; Yanai and Endo, 2021). Quantification with the lysosomal probe revealed that lysosomal activity in hippocampal NSCs 1) increases in a quiescent state, 2) increases from the juvenile period to adolescence, 3) remains stable in adults, and 4) decreases with age and due to Alzheimer's disease pathogenesis (Oakley et al., 2006). These three different stages of lysosomal degradation activity suggest different roles for lysosomes in NSC maintenance in the brain.

Results and Discussion

Lysosomal probe to monitor protein degradation in lysosomes

To monitor lysosomal activity at the single-lysosome resolution *in vivo*, we generated a new variant of the Lysosomal-METRIQ (Measurement of protein Transporting integrity by RatIo Quantification) probe (Ishii et al., 2019). Our probe comprises lysosomal deoxyribonuclease (DNase) II alpha fused in tandem to two fluorescent proteins, mCherry and super-folder green fluorescent protein (sfGFP) (Khmelinskii et al., 2012). DNase II alpha is a lysosomal enzyme which is synthesized in the endoplasmic reticulum (ER) and transported to lysosomes via the Golgi apparatus (Ohkouchi et al., 2013). Our probe, called LysoMonitor (LyMo), is a tandem-fusion protein with short linker peptides between DNase II alpha and two fluorescent proteins (Fig. 1A), which have different stabilities at low pH and toward lysosomal proteases. While mCherry is stable in lysosomes (half-life > 1 day), sfGFP is comparatively unstable (half-life 2.8 hours in Fig. 1E) (Katayama et al., 2008; Pedelacq et al., 2006). LyMo signals in NSCs were compared by immunostaining. Lysosomal marker Lamp1 colocalized fully with mCherry signals, and GFP signals were distributed diffusely in cells but colocalized with weaker mCherry signals than those in lysosomes because LyMo was transported into lysosomes via the ER and Golgi (Fig. 1B; Fig. S1A, B). This suggests that,

compared with mCherry, the GFP moiety of LyMo is unstable and degrades rapidly after being transported into lysosomes, which are regions with strong mCherry signals (Fig. S1A). GFP and mCherry signal intensities were measured in thresholded mCherry "dots" representing lysosomes. Lysosomal activity was calculated by dividing GFP intensity by mCherry intensity within each dot (Fig. 1C).

The lysosomal inhibitor bafilomycin A1 (BafA) increased the GFP to mCherry signal ratio, while the mTORC1 kinase inhibitor Torin1 (Settembre et al., 2012) activated lysosomes by activating TFEB and decreased the GFP to mCherry signal ratio (Fig. 1B, C; Fig. S1C, D). These results support an inverse correlation between the GFP to mCherry signal ratio and lysosomal activity (Fig. 1 A, C). To verify the degradation of LyMo in lysosomes, the stabilities of GFP and mCherry were determined by cycloheximide-chase experiments and western blotting. Cycloheximide is a protein synthesis inhibitor, and the cycloheximide-chase can measure the protein kinetics and stability without the effect of newly synthesized protein. We found that 1) the GFP and mCherry fusion components were excised from full length LyMo (upper bands ~50 kDa (mCherry-GFP fusion) and ~100 kDa (full length) in Fig. 1D; Fig. S1E), 2) the excised mCherry was stable, and 3) the excised GFP was rapidly degraded (mCherry and GFP bands at ~25 kDa in Fig. 1D). GFP degradation depended on lysosomal activity and was inhibited by BafA (Fig. 1D, E). These results indicate that the calculated ratio of LyMo signals detected by immunostaining for GFP and mCherry reflects proteolytic activity in the lysosome.

LyMo transgenic mice to monitor lysosomal activity *in vivo*

LyMo was applied to monitor lysosomal activity *in vivo* by immunostaining using transgenic (Tg) mice. To express LyMo in NSCs of the mouse brain, we generated Tg mice expressing LyMo under the control of the mouse glial fibrillary acidic protein (GFAP) promoter (Fig. 2A), which is active in adult NSCs and astrocytes (Seki et al., 2014). In the hippocampal dentate gyrus (DG), mCherry signals of LyMo were present in the granular cell layer and colocalized with Lamp1 (Fig. 2B, right panels). These mCherry dots were present in cells that were positive for NSC markers: Sox2, GFAP, and Nestin (Fig. 2B, left and center panels). To verify that these LyMo signals can be used to quantify lysosomal activity in brain tissue, DG brain slices were immunostained with antibodies against GFP and mCherry, and simultaneously stained with DAPI following slice culture in lysosomal inhibitor, BafA, or lysosomal activator, Torin 1(Fig. 2C, D; Fig. S1F). Based on GFP and mCherry intensities in the DG, we observed an increased ratio of GFP to mCherry in the presence of the lysosomal inhibitor, BafA (Fig.

2D). On the other hand, Torin 1 reduced the ratio of GFP to mCherry (Fig. S1F). From these results, we deduced that relative lysosomal activity in tissue can be monitored accurately by quantifying LyMo using immunohistochemistry.

Using LyMo mice, we compared lysosomal activity in proliferating and quiescent NSCs in mouse brains at the age of two weeks (P14) since there were many proliferating Ki-67+ NSCs at this age (Fig. 2E, Fig. S4A). To identify LyMo signals in individual NSCs, radial-shaped NSCs were segmented using Sox2 (nuclear) and GFAP (cytoplasmic) signals. Ki-67 signals were used to distinguish proliferating NSCs (Fig. 2E). LyMo dots in individual NSCs were quantified. Results demonstrated that lysosomal proteolytic activity *in vivo* was higher in quiescent NSCs than in proliferating NSCs, even with individual variations (Fig. 2F, Fig. S2). This result is consistent with our previous report that lysosomal degradation is enhanced in quiescent NSCs (Kobayashi et al., 2019), although it would be technically challenging to compare all lysosomal activities in individual cells because lysosomes are present throughout NSCs, namely in the soma, axon, and dendrites.

We proceeded to investigate lysosomal activity in the adult mouse brain NSCs after their activation by voluntary running since physical exercise has been shown to activate neurogenesis in the hippocampus (Garrett et al., 2012; van Praag et al., 1999). Transgenic young adult mice expressing LyMo were divided into individual cages either with or without free access to a running wheel for six weeks. Immunohistochemistry detected both an increase of approximately 2% (from 13.8% to 15.9%) of Ki-67-positive proliferating cells among Sox2-positive cells and an increase in newly born neurons (from 16.4% to 22.7%) that were positive for both Ki-67 and DCX, an immature neuron marker, in the DG of Tg mice in cages with a wheel (Fig. 3A, B; Fig. S3A, B). These results are consistent with previous reports suggesting that physical exercise increases the efficiency of the production of newly born neurons in the adult hippocampus.

Next, we investigated lysosomal activity in NSCs. Since the GFAP promoter is active in both NSCs and astrocytes, we immunostained with S100β, an astrocyte marker antibody, to separate the LyMo signals from astrocytes for measurement. S100β-positive cells were present in the DG even if LyMo-positive cells have a radial glia-like morphology, which is typical for NSCs in the DG (Fig. 3C, lower panels; Fig. 3D) (Karpf et al., 2022; Kriegstein and Alvarez-Buylla, 2009). LyMo signals in S100β-negative and -positive cells were quantified to calculate lysosomal activity in NSCs and astrocytes in the DG, respectively. Quantification revealed increased lysosomal activity in the hippocampal DG of mice in wheel cages for both NSCs and

astrocytes because GFP/mCherry ratios in running mice were lower than those in control mice (Fig. 3E, Fig. S3C). These results indicate that exercise enhances neurogenesis in the hippocampus, which is accompanied by an increase in lysosomal activity in both NSCs and astrocytes. Lysosomal activation in astrocytes and NSCs implies that the global changes occurred in the brain, such as those previously reported beneficial effects on vascular systems, which are severely damaged by the aging process in the brain (Cole et al., 2022), or by the enhanced brain metabolic systems with increased growth factors, nutrients, and energy supply (Cotman et al., 2007). The results are consistent with findings that exercise increases the expression of lysosomal-related proteins in the brain after running through TFEB activation *in vivo* (Huang et al., 2019). Increased lysosomal activity in both NSCs and astrocytes implies that an enhanced vascular function caused by physical exercise alters the metabolic state and increases overall lysosomal activity (Leiter et al., 2019).

Lysosomal activity fluctuation depends on maturation, age, and disease *in vivo*

Previous reports have shown that lysosomes contribute to the differentiation, quiescence, and aging of NSCs (Kobayashi et al., 2019; Leeman et al., 2018; Yuizumi et al., 2021). In addition, lysosomal dysfunction with lowered v-ATPase activity in neurons was recently reported to precede the onset of neurodegeneration associated with Alzheimer's disease (Lee et al., 2022). Therefore, we went on to investigate changes in lysosomal activity in NSCs upon brain maturation, aging, and disease. First, we analyzed the activity state of NSCs in proliferation and neurogenesis in the brain of mice from the juvenile stage (two weeks old) to old age (two years old). Thirty-four percent of Sox2-positive NSCs were double-positive for Ki-67 at two weeks of age but decreased markedly with age in the hippocampal DG. A similar decrease was observed in 5xFAD mice (Fig. 4A; Figs. S4A, S5A). DCX-positive immature neuron production was reduced in two-month-old 5xFAD mice compared with control healthy mice (9.2% in controls and 7.3% in 5xFAD mice; p-value < 0.0001), but did not differ significantly at either six months or one year (Fig. 4B; Figs. S4B, S5B). These results suggest that age-dependent reductions in both proliferation and neurogenesis are predominant to disease-dependent ones in this time series. Neurogenesis was mainly affected by age in the adult brain in these transgenic mice.

Next, we quantified lysosomal activity using LyMo in hippocampal NSCs in these mice (Fig. 4C, Fig. S6). Lysosomal activity increased from age two weeks (P14) to two months (2M), increased slightly from age two months to six months, and subsequently decreased from one year to two years of age (Fig. 4D). In 5xFAD mice, a

decrease in lysosomal activity was observed between two and six months of age (Fig. 4D). These results demonstrated that lysosomal activity increased with brain maturation and was inversely correlated with the proliferation and differentiation potentials of NSCs from juvenile (two weeks old) to adult periods (two and six months old) even with individual variations (Fig. S5C). However, this relationship was disrupted by both further aging and disease; lysosomal activity suddenly decreased in NSCs at one and two years in control wild-type mice and decreased earlier, between two and six months old, in 5xFAD mice than in the control mice (Fig. 4E). Conversely, lysosomal activity in astrocytes of the hippocampal DG of non-diseased control mice increased from two weeks to six months of age, similarly to NSCs, and decreased after six months to slightly less in astrocyte than that in NSCs (Fig. 4F, G). This result suggests that lysosomal activity was still maintained to some extent in astrocytes in aged mouse brains. However, in 5xFAD mice, lysosomal activity was reduced transiently at six months but recovered at one year of age. This change was puzzling as higher lysosomal activity at an older age (two years old), but the findings may suggest that disease-dependent damage, for instance, the accumulation of amyloid-β plaques, reduces lysosomal activity at first; however, lysosomal activity later increases in response to this damage via astrocyte activation. Finally, the expression levels of LyMo were compared in individual mice (Fig. S7). The results showed that the expression levels of LyMo were variable in individual mice, and the mCherry intensity means indicate no genotype or age dependency with LyMo expression in NSCs and astrocytes in our analyses.

Our method of measuring *in vivo* lysosomal activity using LyMo mice revealed that the fluctuation of lysosomal activity in NSCs depends on brain maturation, age, disease stage, and physical exercise. Lysosomal activity has been detected through the quenching of GFP fluorescence due to the relatively lower pH in lysosomes; however, our new probe, LyMo, enabled us to monitor the "protein degradation" of destabilized GFP in lysosomes. Moreover, our method enables lysosomal activity to be measured in NSCs of the hippocampal DG with spatial information and characterization by IHC. Ours is the first report to monitor the fluctuation of lysosomal protein degradation activity in NSCs *in vivo*. Our measurements suggest that lysosomal activity may serve as an early and sensitive indicator of cellular condition in the brain along life stages. This method could also be applied to other tissues as well to measure lysosomal activity and cellular state *in vivo*.

Materials and methods

Cell culture. NSCs were grown in DMEM/F-12 (Gibco) supplemented with 20 ng/ml EGF (Wako), 20 ng/ml bFGF (Wako), P/S (Nacalai Tesque), and N-2 max media supplement (R&D) (Kobayashi et al., 2019) without any contamination. NSCs expressing LyMo were generated by lentiviral transduction with a Tet-On inducible cassette (Ishii et al., 2019; Kobayashi et al., 2019) and incubated for one day in the presence of doxycycline. Inhibitors were used at the following concentrations: 20 nM bafilomycin A1 (Sigma), 100 nM Torin 1 (Cayman Chemical), and 10 µg/ml cycloheximide (Sigma). For immunocytochemistry, cells were fixed in 4% PFA/PBS on ice, permeabilized with 0.1% Triton X-100 in PBS (PBST), blocked in 5% normal goat serum/PBST, and stained with antibodies in 1% normal goat serum/PBST. For western blotting, cells were first lysed in lysis buffer (50 mM Tris-HCl [pH 8.0], 100 mM NaCl, 5 mM $MgCl_2$, 0.5% Nonidet P-40, protease inhibitor cocktail (Roche), 1 mM phenylmethylsulfonyl fluoride, 250 U/ml Benzonase (Sigma), and phosphatase inhibitors) on ice after washing with cold PBS. Cell lysates were later subjected to SDS-PAGE followed by western blotting onto a PVDF membrane (Immobilon-P; Millipore).

Mice. Mice were maintained in our animal facility and under a 12:12 hour light–dark cycle. Animal care and experiments were conducted per animal experiment committee guidelines of Kyoto University and the University of Tokyo. Additionally, we complied with all relevant ethical animal testing and research regulations. LyMo Tg mice were created by injecting fertilized eggs from the C57BL/6 mice with DNA constructs containing the mouse GFAP promoter, lysosomal probe-coding sequences, and rabbit β-globin polyadenylation signal. For voluntary running experiments, the Tg mice were housed individually in cages with or without a running wheel at six weeks old and sacrificed after six weeks. In addition, 5XFAD Tg mice were obtained from the Jackson Laboratory (#034840-JAX B6SJL-Tg (APPSwFlLon, PSEN1*M146L*L286V) 6799Vas/Mmjax) and crossed with LyMo mice to make double Tg mice. Age detail is described in the figure legends. Sex was not considered in this study.

Brain sample preparation. For immunohistochemistry of the brain's DG, mice were transcardially perfused with 4% PFA/PBS. Brains were post-fixed in 4% PFA/PBS, cryoprotected with sucrose/PBS, embedded, and frozen in OCT compound (Tissue TEK). Fixed brains were cryosectioned with 20 µm thickness. Every twelfth slice of 20 µm cryosections taken along the caudal-rostral axis throughout the entire DG was

immunostained for quantification. For slice culture, brains were dropped into cutting solution (280 mM sucrose, 2 mM KCl, 10 mM HEPES-NaOH [pH 7.4], 0.5 mM CaCl$_2$, 10 mM MgCl$_2$, and 10 mM glucose) and sectioned into 200 µm-thick slices on a vibratome (Leica, VT1200S; Dosaka EM, Neo-LinearSlicer AT). Brain slices were incubated in bath solution (135 mM NaCl, 5 mM KCl, 1 mM CaCl$_2$, 1 mM MgCl$_2$, 10 mM HEPES-NaOH [pH 7.4], and 10 mM glucose) for 30 min while oxygen was bubbled into the solution before being transferred on to Millicell Cell Culture Inserts (0.4-µm pore size, EMD Millipore) covered with Cellmatrix Type I-A collagen gel (Nitta Gelatin). Inserts were incubated overnight in the culture medium (10% FBS/ bath solution) with either bafilomycin A1 added or not. Slices were fixed with 4% PFA/PBS for 1 h and immunostained after being removed from the collagen gel. Three to six slices were measured per condition.

Antibodies. Chicken anti-GFP (Abcam, ab13970), goat anti-mCherry (SICGEN, AB0040), rat anti-Lamp1 (Developmental Studies Hybridoma Bank, 1D4B), mouse anti-GFAP (sigma, G3893), goat anti-Sox2 (R&D Systems, AF2018), chicken anti-Nestin (aves, NES), rabbit anti-S100β (Abcam, ab52642), rat anti-Ki-67 (eBioscience, SolA15), and rabbit anti-DCX (CST, 4604) antibodies were used for immunohistochemistry and immunocytochemistry. Rabbit anti-GFAP (sigma, G9269) and rabbit anti-Sox2 (Millipore, AB5603) antibodies were used to make the NSC surface by using the same 2nd antibody. Rabbit anti-GFP (Thermo, A11122), rabbit anti-mCherry (Abcam, ab167453), and rabbit anti-β-actin (Sigma, A2066) antibodies were used for western blotting. In addition, we used either donkey or goat antibodies conjugated with Alexa 488, 568, or 647 (Thermo, Abcam) and goat antibodies conjugated with HRP (GE) as secondary antibodies.

IHC. Brain cryosections were incubated in Histo-VT one (Nakalai) at 70 °C for 20 min before permeabilization and blocking with 5% normal donkey serum (NDS)/0.1% Triton X-100/PBS (PBST). Cryosections were subsequently stained with 1st and 2nd antibodies as well as DAPI (Sigma) in PBST. Aged brain samples (2Y) were treated with an autofluorescence eliminator reagent (Millipore) to reduce lipofuscin-related background. Following slice culture, brain slices were permeabilized with 0.3% Triton X-100/PBS before they were blocked in 5% normal donkey serum (NDS)/0.3% Triton X-100/PBS, and stained with 1st and 2nd antibodies in 1% NDS/0.3% Triton X-100/PBS. Confocal z-stack images were obtained using a Stellaris 5 (Leica) and LSM880 Airyscan (Zeiss).

Counting proliferating NSCs and newly born neurons. Imaris Cell Imaging Software (Oxford Instruments) was used for all counting using 3D confocal images. Sox2, DCX, and Ki-67 were masked by the DAPI surface (5 µm surface detail) to extract cells in the granular cell layer of the DG. Spots were put on Sox2-positive (XY diameter 5µm, signals with both max intensity above 2500 and mean intensity above 700) and DCX-positive (XY diameter 10 µm, signals with quality above 1000) areas for counting. Ki-67 intensity (intensity standard deviation above 2700) was used to filter the spots for counting Ki-67-Sox2 and Ki-67-DCX double-positive cells.

Quantification of lysosomal activity by LyMo. In cells after immunocytochemistry, spots for measurement were detected as mCherry-positive dots of lysosomes with 0.8 µm diameter and 6000 quality value using Imaris Cell Imaging Software. mCherry and GFP intensity within these spots were measured, and GFP intensity was divided by mCherry intensity; the resulting ratio was normalized to the median value of the control sample. During western blotting of NSCs, both LyMo full-length and GFP-mCherry fusion was detected by both GFP and mCherry antibodies at 100 kDa and 50 kDa. GFP, mCherry, and β-actin band intensities were quantified individually on a LAS3000 image analyzer (Fujifilm) and normalized to the corresponding intensity of the β-actin band. In brain tissues subjected to immunohistochemistry, mCherry and S100β signals were masked by the surface generated from DAPI staining of the granular cell layer (DAPI-mask). Spots for measurements were placed on mCherry-positive lysosomal signals with 2 µm diameter. mCherry spots were filtered by "quality" and the top 2 % of spots were analyzed. To isolate S100β-positive astrocytes, an additional S100β surface was generated within the DAPI-mask using S100β signals (1.14 µm surface detail), distinguishing mCherry spots inside and outside the distance value from the S100β surface. The ratio of GFP to mCherry intensity was calculated with Python. In single-cell LyMo measurements *in vivo*, after masking all the channels by the DG region drawn manually, the NSC surface was made from the signals of both Sox2 and GFAP (0.5 µm surface detail, 1800 quality value) obtained rabbit Sox2 and GFAP antibodies, and masked all signals again. Proliferating and quiescent NSCs were classified by Ki-67 signals.

Statistical analysis. Statistical analyses were performed using Prism 8 and 10 (GraphPad Software). Statistical differences were examined using Student's t-test, one-way ANOVA, and two-way ANOVA with Tukey's multiple comparisons tests and nested one-way ANOVA; p-values < 0.05 were considered significant.

Author contributions: HZ, KI, and TK conducted all experiments. TS performed data processing on results from LyMo mice. SI and EI established the construct of the LyMo probe. MH and ZL helped ZH with mouse experiments. RT established the NSC line expressing LyMo. SK and HM helped to obtain transgenic mice by *in vitro* fertilization. RK provided 5xFAD mice. TK designed the experiments and wrote the manuscript; KI performed English language editing.

References

Ballabio, A. and Bonifacino, J. S. (2020). Lysosomes as dynamic regulators of cell and organismal homeostasis. *Nat Rev Mol Cell Biol* **21**, 101-118.

Cole, J. D., Sarabia Del Castillo, J., Gut, G., Gonzalez-Bohorquez, D., Pelkmans, L. and Jessberger, S. (2022). Characterization of the neurogenic niche in the aging dentate gyrus using iterative immunofluorescence imaging. *Elife* **11**, e68000.

Cotman, C. W., Berchtold, N. C. and Christie, L. A. (2007). Exercise builds brain health: key roles of growth factor cascades and inflammation. *Trends Neurosci* **30**, 464-472.

Fuentealba, L. C., Obernier, K. and Alvarez-Buylla, A. (2012). Adult neural stem cells bridge their niche. *Cell Stem Cell* **10**, 698-708.

Furutachi, S., Miya, H., Watanabe, T., Kawai, H., Yamasaki, N., Harada, Y., Imayoshi, I., Nelson, M., Nakayama, K. I., Hirabayashi, Y. et al. (2015). Slowly dividing neural progenitors are an embryonic origin of adult neural stem cells. *Nat Neurosci* **18**, 657-665.

Garrett, L., Lie, D. C., Hrabe de Angelis, M., Wurst, W. and Holter, S. M. (2012). Voluntary wheel running in mice increases the rate of neurogenesis without affecting anxiety-related behaviour in single tests. *BMC Neurosci* **13**, 61.

Huang, J., Wang, X., Zhu, Y., Li, Z., Zhu, Y. T., Wu, J. C., Qin, Z. H., Xiang, M. and Lin, F. (2019). Exercise activates lysosomal function in the brain through AMPK-SIRT1-TFEB pathway. *CNS Neurosci Ther* **25**, 796-807.

Ishii, S., Matsuura, A. and Itakura, E. (2019). Identification of a factor controlling lysosomal homeostasis using a novel lysosomal trafficking probe. *Sci Rep* **9**, 11635.

Karpf, J., Unichenko, P., Chalmers, N., Beyer, F., Wittmann, M. T., Schneider, J., Fidan, E., Reis, A., Beckervordersandforth, J., Brandner, S. et al. (2022). Dentate gyrus astrocytes exhibit layer-specific molecular, morphological and physiological features. *Nat Neurosci* **25**, 1626-1638.

Katayama, H., Yamamoto, A., Mizushima, N., Yoshimori, T. and Miyawaki, A. (2008). GFP-like proteins stably accumulate in lysosomes. *Cell Struct Funct* **33**, 1-12.

Khmelinskii, A., Keller, P. J., Bartosik, A., Meurer, M., Barry, J. D., Mardin, B. R., Kaufmann, A., Trautmann, S., Wachsmuth, M., Pereira, G. et al. (2012). Tandem fluorescent protein timers for in vivo analysis of protein dynamics. *Nat Biotechnol* **30**, 708-714.

Kobayashi, T., Piao, W., Takamura, T., Kori, H., Miyachi, H., Kitano, S., Iwamoto, Y., Yamada, M., Imayoshi, I., Shioda, S. et al. (2019). Enhanced lysosomal degradation maintains the quiescent state of neural stem cells. *Nat Commun* **10**, 5446.

Kriegstein, A. and Alvarez-Buylla, A. (2009). The glial nature of embryonic and adult neural stem cells. *Annu Rev Neurosci* **32**, 149-184.

Lee, J. H., Yang, D. S., Goulbourne, C. N., Im, E., Stavrides, P., Pensalfini, A., Chan, H., Bouchet-Marquis, C., Bleiwas, C., Berg, M. J. et al. (2022). Faulty autolysosome acidification in Alzheimer's disease mouse models induces autophagic build-up of Abeta in neurons, yielding senile plaques. *Nat Neurosci* **25**, 688-701.

Leeman, D. S., Hebestreit, K., Ruetz, T., Webb, A. E., McKay, A., Pollina, E. A., Dulken, B. W., Zhao, X., Yeo, R. W., Ho, T. T. et al. (2018). Lysosome activation clears aggregates and enhances quiescent neural stem cell activation during aging. *Science* **359**, 1277-1283.

Leiter, O., Seidemann, S., Overall, R. W., Ramasz, B., Rund, N., Schallenberg, S., Grinenko, T., Wielockx, B., Kempermann, G. and Walker, T. L. (2019). Exercise-Induced Activated Platelets Increase Adult Hippocampal Precursor Proliferation and Promote Neuronal Differentiation. *Stem Cell Reports* **12**, 667-679.

Mizushima, N. and Murphy, L. O. (2020). Autophagy Assays for Biological Discovery and Therapeutic Development. *Trends Biochem Sci* **45**, 1080-1093.

Morrow, C. S., Porter, T. J., Xu, N., Arndt, Z. P., Ako-Asare, K., Heo, H. J., Thompson, E. A. N. and Moore, D. L. (2020). Vimentin Coordinates Protein Turnover at the Aggresome during Neural Stem Cell Quiescence Exit. *Cell Stem Cell* **26**, 558-568 e559.

Neefjes, J. and Dantuma, N. P. (2004). Fluorescent probes for proteolysis: tools for drug discovery. *Nat Rev Drug Discov* **3**, 58-69.

Oakley, H., Cole, S. L., Logan, S., Maus, E., Shao, P., Craft, J., Guillozet-Bongaarts, A., Ohno, M., Disterhoft, J., Van Eldik, L. et al. (2006). Intraneuronal beta-amyloid aggregates, neurodegeneration, and neuron loss in transgenic mice with five familial Alzheimer's disease mutations: potential factors in amyloid plaque formation. *J Neurosci* **26**, 10129-10140.

Ohkouchi, S., Shibata, M., Sasaki, M., Koike, M., Safig, P., Peters, C., Nagata, S. and Uchiyama, Y. (2013). Biogenesis and proteolytic processing of lysosomal DNase II. *PLoS One* **8**, e59148.

Pedelacq, J. D., Cabantous, S., Tran, T., Terwilliger, T. C. and Waldo, G. S. (2006). Engineering and characterization of a superfolder green fluorescent protein. *Nat Biotechnol* **24**, 79-88.

Seki, T., Sato, T., Toda, K., Osumi, N., Imura, T. and Shioda, S. (2014). Distinctive population of Gfap-expressing neural progenitors arising around the dentate notch migrate and form the granule cell layer in the developing hippocampus. *J Comp Neurol* **522**, 261-283.

Settembre, C., Zoncu, R., Medina, D. L., Vetrini, F., Erdin, S., Erdin, S., Huynh, T., Ferron, M., Karsenty, G., Vellard, M. C. et al. (2012). A lysosome-to-nucleus signalling mechanism senses and regulates the lysosome via mTOR and TFEB. *EMBO J* **31**, 1095-1108.

Urban, N. and Guillemot, F. (2014). Neurogenesis in the embryonic and adult brain: same regulators, different roles. *Front Cell Neurosci* **8**, 396.

van Praag, H., Kempermann, G. and Gage, F. H. (1999). Running increases cell proliferation and neurogenesis in the adult mouse dentate gyrus. *Nat Neurosci* **2**, 266-270.

Yanai, S. and Endo, S. (2021). Functional Aging in Male C57BL/6J Mice Across the Life-Span: A Systematic Behavioral Analysis of Motor, Emotional, and Memory Function to Define an Aging Phenotype. *Front Aging Neurosci* **13**, 697621.

Yuizumi, N., Harada, Y., Kuniya, T., Sunabori, T., Koike, M., Wakabayashi, M., Ishihama, Y., Suzuki, Y., Kawaguchi, D. and Gotoh, Y. (2021). Maintenance of neural stem-progenitor cells by the lysosomal biosynthesis regulators TFEB and TFE3 in the embryonic mouse telencephalon. *Stem Cells* **39**, 929-944.

Figures
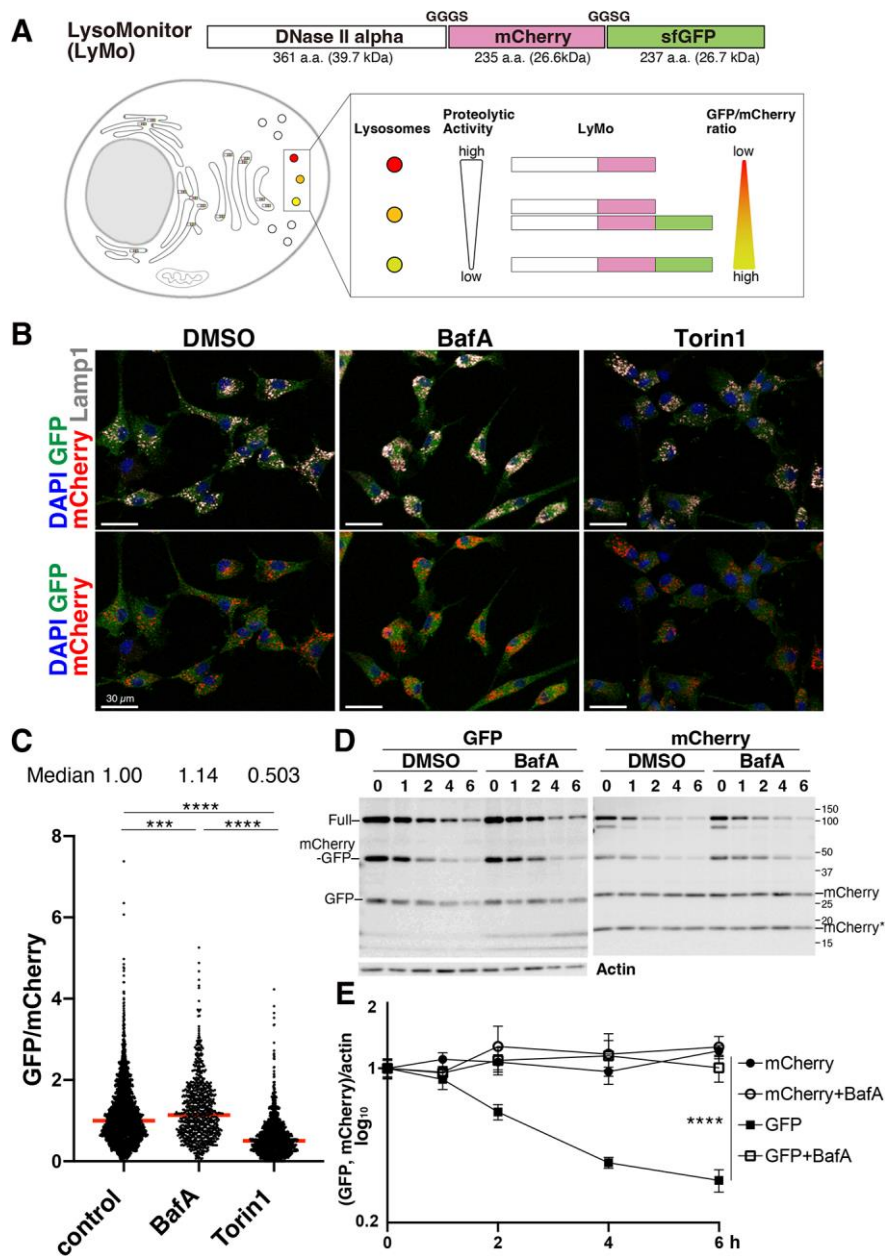
Fig.1. A novel lysosomal probe for monitoring protein degradation in lysosomes.
A. Lysosome monitoring probe (LysoMonitor, LyMo). Schematic illustration of LyMo and the correlation between lysosomal proteolytic activity and GFP/mCherry ratio. **B. LyMo immunofluorescence imaging.** NSCs expressing LyMo were immunostained for GFP (green), mCherry (red), and Lamp1 (grey) with DAPI (blue). NSCs were cultured with doxycycline for one day to induce LyMo expression using a

Tet-on system and incubated with either DMSO, 20 nM bafilomycin A1(BafA), or 100 nM Torin1 for 4 h. Scale bars, 30 μm. **C. Quantification of LyMo.** GFP intensity divided by mCherry intensity was measured in mCherry-positive individual lysosomes and normalized to the control sample median (two replicates; total cell number is 181 (DMSO), 93 (BafA) and 340 (Torin1); total dot number of mCherry-positive lysosomes for quantification is 2288 (DMSO), 831 (BafA) and 1294(Torin1)). Red bars represent medians. (***$p < 0.001$, ****$p < 0.0001$; one-way ANOVA with Tukey's multiple comparisons tests). Median values are indicated above the chart. **D, E. Protein stability of LyMo.** NSCs expressing LyMo incubated with cycloheximide with or without 20 nM bafilomycin A1 (BafA). Full-length LyMo and mCherry-sfGFP fusion proteins were commonly detected with GFP- and mCherry-specific antibodies at around 100 and 50 kDa, respectively (D). GFP and mCherry bands around 25 kDa (noted as GFP and mCherry in panel D) were measured and plotted in the chart after normalization to actin (E). Truncated mCherry (indicated as mCherry* around 20 kDa) was not used for measurement. Data represent means ± s.e.m. (****$p < 0.0001$; two-way ANOVA with Tukey's multiple comparison tests, n = 4).
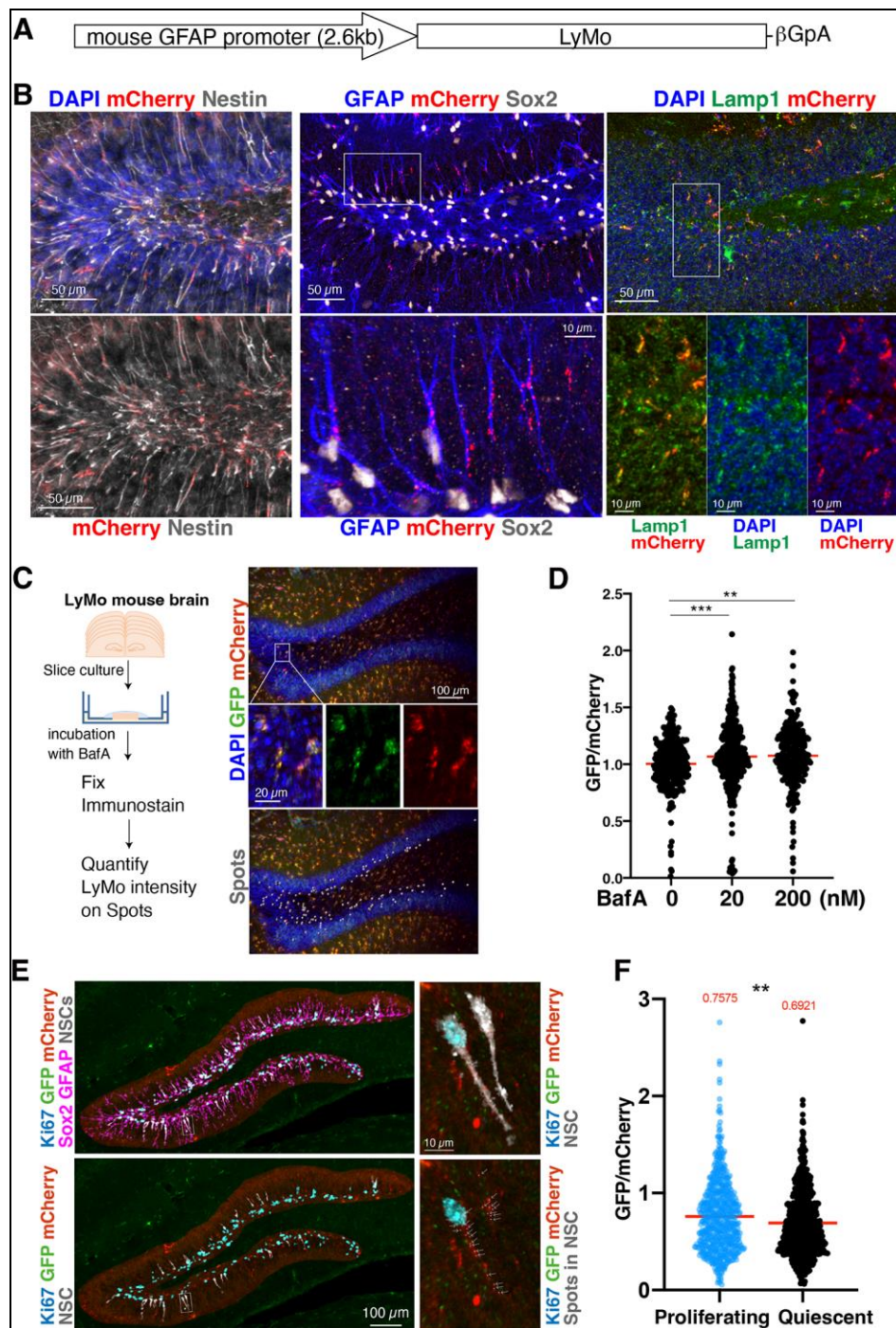
Fig. 2. Transgenic mice for monitoring lysosomal degradation activity in NSCs of brain tissue.

A. Schematic of LyMo construct for transgenic mice. B. LyMo expression in the DG. Left: Nestin (grey)-positive NSCs express LyMo (mCherry, red). Middle: GFAP (blue) and Sox2 (grey)-positive NSCs with radial fiber express LyMo (mCherry, red).

Right: LyMo expression (mCherry) colocalizes with Lamp1 (green). The area enclosed by the white squares was enlarged in the lower panels. No fluorescence signal of LyMo was detected without IHC (not shown). **C. Slice culture of LyMo mouse brain (C).** Left: Schematic representation of the experimental flow. Brain slices from LyMo mouse at 14 months of age were cultured with or without bafilomycin A1 (BafA) present for one day. Right: representative image of IHC (upper), enlarged images (middle), and measurement (lower). Spots (grey in the lower panel) were put on mCherry dots in the granule cell layer (DAPI) to measure LyMo intensity in NSCs. **D. Quantification of LyMo brain slices.** GFP and mCherry ratio was measured in mCherry dots and normalized to the median for the control sample. Red bars represent medians. (**$p <$ 0.01, ***$p <$ 0.001; one-way ANOVA with Tukey's multiple comparisons tests, n = 3 (slices)). **E. Separation of proliferating and quiescent NSCs.** The area of the molecular layer and the SGZ were traced by hand and masked (left panels). Radial-shaped NSCs (grey) and proliferating NSCs were identified from Sox2 and GFAP staining (magenta in the upper left panel) and the Ki67 staining (blue), respectively. The area enclosed by the white squares in the left panels was enlarged in the right panels with spots of LyMo for measurement (white arrows, the right lower panel). **F. LyMo quantification in proliferating and quiescent NSCs.** Red bars and the upper values represent medians. (**$p <$ 0.01; Student's t-tests, n=75 (proliferating cells, blue) and 86 (quiescent cells, black) from three mice at P14).
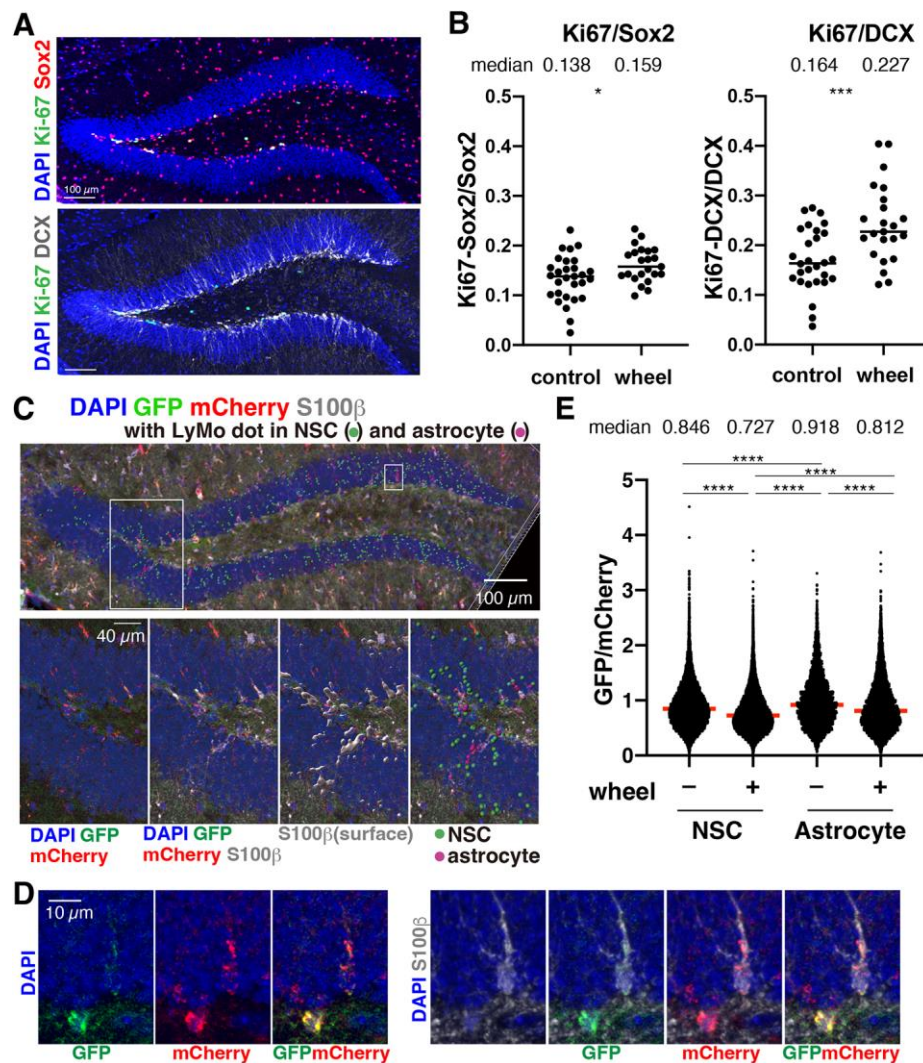
Fig. 3. Lysosomal activity in NSCs of the DG of mice with or without running wheel.

A. Measurement of proliferating NSCs and newly born neurons. Representative photos for counting proliferating Ki-67+ (green)/Sox2+ (red) cells and Ki-67+ (green)/DCX+ (grey) cells in the DG. Ki-67+/Sox2+ cells are white in the upper panel.

B. Proliferating cells in the DG of mice. The ratio of Ki-67+/Sox2+ to Sox2+ cells (left) and Ki-67+/DCX+ to DCX+ cells were calculated and plotted. Each data point represents results from one brain section. Bars represent median values. (*$p < 0.05$, ***$p < 0.001$; Student's t-test). Median values are above the chart. **C.D. LyMo measurement in NSCs of the hippocampal DG.** Spots correspond to mCherry (red)-positive lysosomes in the molecular layer of the DG (DAPI, blue). The grey surface is the S100β positive area. Magenta and green spots are mCherry of LyMo in S100β positive (astrocyte) and negative cells (NSC), respectively. The area enclosed by

the white squares was enlarged in the lower panels in (C) and (D). **E. Activation of lysosomal protein degradation in the DG.** GFP and mCherry ratio was measured in spots (C) and adjusted with the median of the control sample (2M wild type in Fig. 4E). Red bars represent medians. (****$p < 0.0001$; one-way ANOVA with Tukey's multiple comparison tests, n = 6). Median values are above the chart.
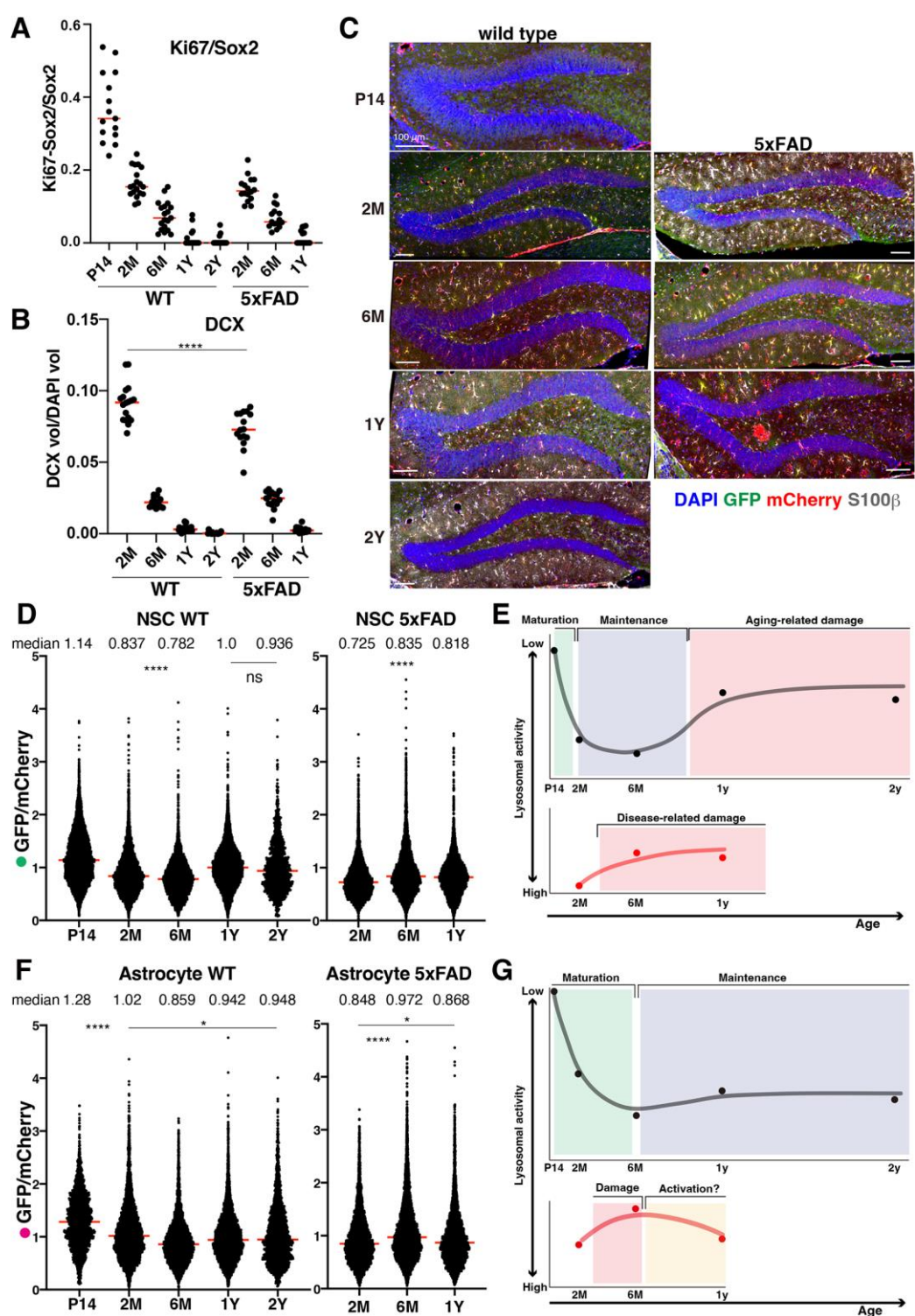
Fig. 4. Lysosomal activity fluctuation in NSCs of the DG with age.

A, B. Measurement of proliferating NSCs and early-born neurons in the DG. Ratio of Ki-67+/Sox2+ cells to all Sox2+ cells in the SGZ of the DG (A). DCX-positive volume was divided by the DAPI-positive volume (B). Each data point represents the

result from one brain section. Red bars represent median values. **C. LyMo wild-type and 5xFAD mice of different ages.** Representative images for measuring the lysosomal activity of different age mice and Alzheimer's disease model mice. Scale bars, 100 μm. **D–G. Lysosomal protein degradation activities in NSCs (D) and astrocytes (F) of wild-type and 5xFAD mice and hypothesized models for different lysosomal activity in NSCs (E) and astrocytes (G).** GFP/mCherry ratio was measured and normalized with the median of the control NSCs (wild-type 1Y). Medians are shown as red bars (D, F). All compared pairs showed ****$p < 0.0001$ except some pairs described ns (not significant) or *$p < 0.05$, and median values are above the chart (D, F). Dots in the charts show median values in the wild-type (black lines) and 5xFAD mice (red lines), respectively (E, G).
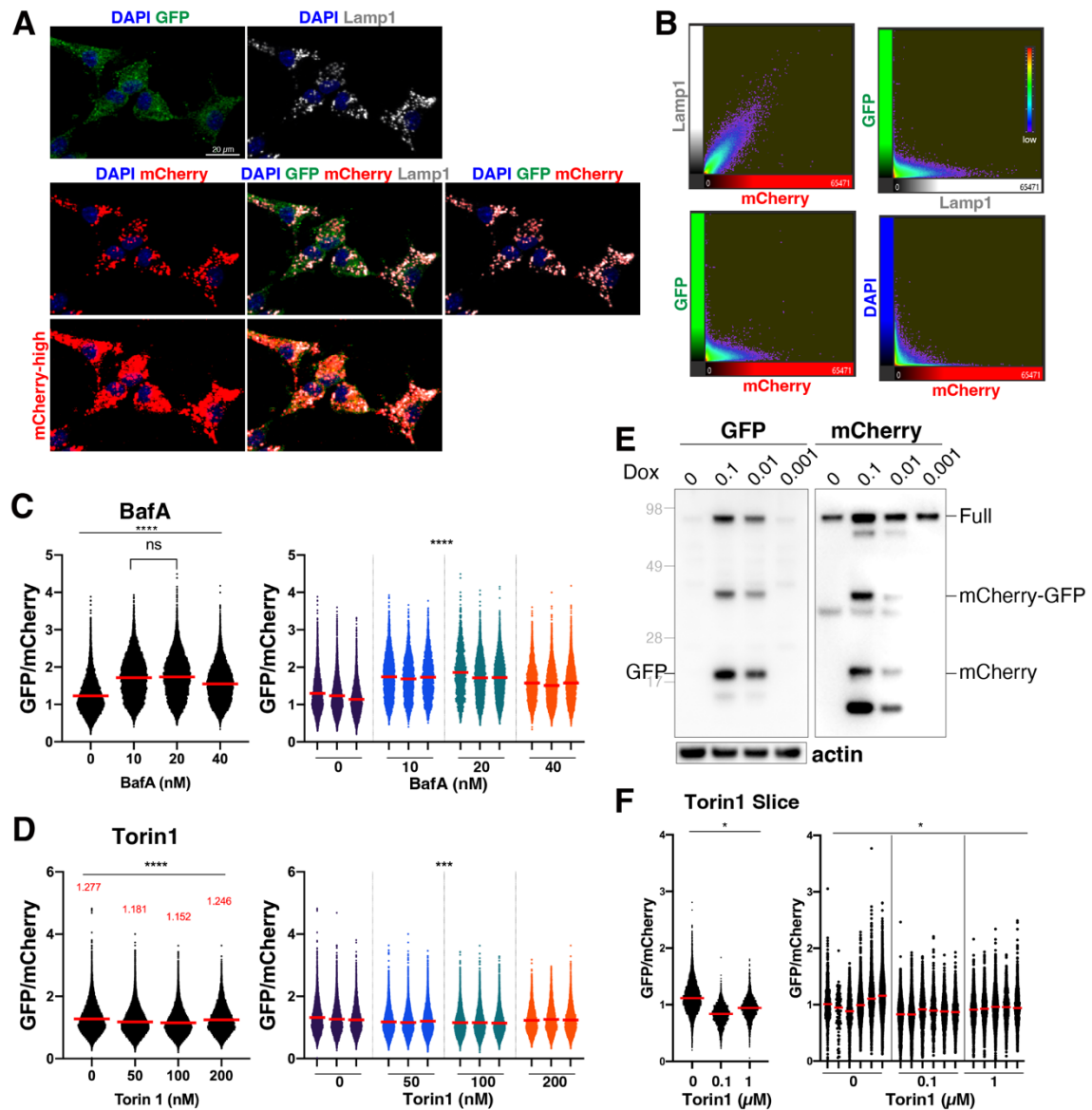
Fig. S1. LyMo expression and dose dependence in NSCs *in vitro*

A. Colocalization of GFP and mCherry signals. Immunocytochemistry of GFP (green), mCherry (red), and Lamp1 (grey) with DAPI (blue) in LyMo-expressing NSCs. GFP signal is diffusively expressed, but mCherry-high signals (lower panels) cover the GFP+ regions. **B. 2D plot of Lamp1, mCherry, GFP, and DAPI intensities.** Plots were created by Imaris Software. mCherry shows a linear correlation with Lamp1 but no correlation with DAPI. **C, D. Dose dependence of BafA (C) and Torin1 (D).** NSCs expressing LyMo were treated with different

concentrations of chemicals and quantified after immunocytochemistry. 10 nM BafA and 50 nM Torin1 changed lysosomal activity for NSCs. 20 nM BafA and 100 nM Torin were appropriate concentrations, but higher concentrations of those chemicals caused damage to cells. Results from the sum and individual data of triplicate samples were shown in the left and right panels, respectively. Red bars and values written in red color represent medians. The total cell number is 1325 for BafA (C) and 1796 for Torin 1 (D), and the total dot number for LyMo measurement is 72479 for BafA (C) and 117488 for Torin 1(D). (***$p < 0.001$, ****$p < 0.0001$; one-way ANOVA (left panels) and nested one-way ANOVA (right panels)). **E. Dose-dependent expression of LyMo induced by doxycycline in NSCs.** NSCs with doxycycline-inducible LyMo were cultured in the presence of doxycycline at 0, 0.1, 0.01, 0.001 µg/ml for one day and subjected to western blotting (Novex® NuPAGE® SDS-PAGE Gel system using 4-12 % Bis-Tris gel) to monitor expression levels of LyMo. We selected 0.1 µg/ml of doxycycline for the concentration of all *in vitro* analyses. **F. Slice culture of LyMo mouse brain with Torin1.** 200µm brain slices from a LyMo mouse at six months old were cultured with 0.1 or 1 µM Torin1, or DMSO overnight and fixed for IHC. Results from the sum and each slice were shown in the left and right panels, respectively. Red bars represent medians. (*$p < 0.05$; nested one-way ANOVA).
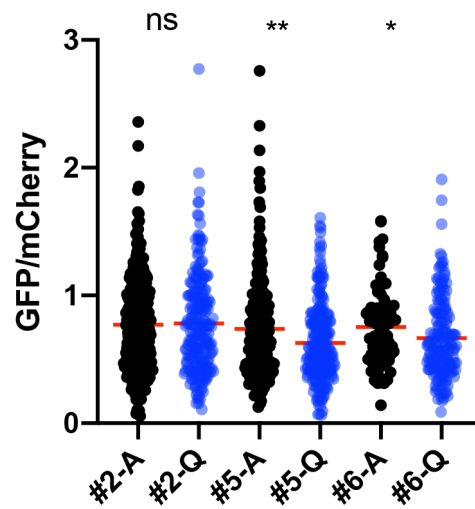
Fig. S2. LyMo measurement of single NSCs *in vivo*

LyMo plots of three individual mice (#2, #5, and #6; P14) corresponding to Fig. 2F. Proliferating cells (A: Active, black) and quiescent (Q, blue) cells were analyzed. Red bars represent medians. (**p* < 0.05,***p* < 0.01; Student's t-tests, ns: not significant).
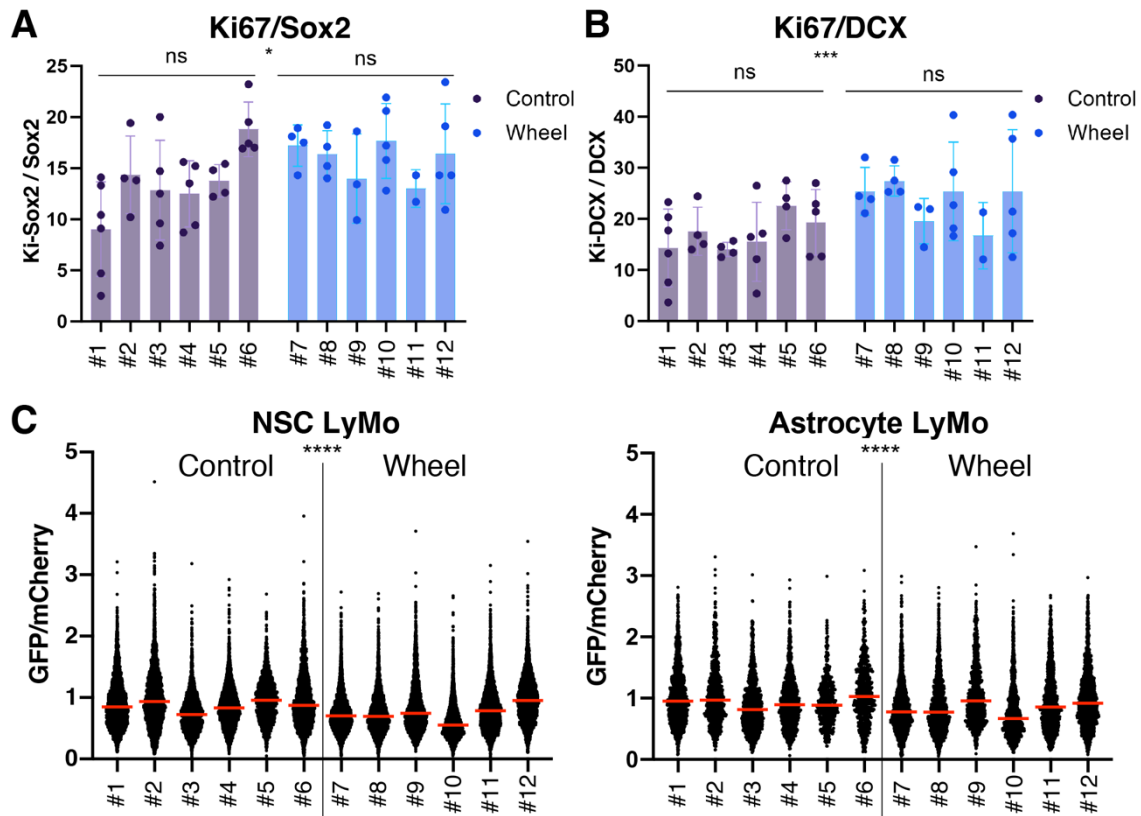
Fig. S3. NSC proliferation, neurogenesis, and lysosomal activity in individual mice with and without running wheel. Measurement plots of proliferating NSCs (**A**; the ratio of Ki-67+/Sox2+ cells to Sox2+ cells), newly born neurons (**B**; the ratio of Ki-67+/DCX to DCX+ cells), and LyMo in NSCs and astrocytes (**C**; GFP and mCherry ratio in mCherry spots of LyMo) of individual mice without (#1–#6) and with (#7–#12) running wheel. These figures correspond to Fig. 3B and E. Red bars represent medians. Bar charts represent means ± s.d. (*$p < 0.05$,***$p < 0.001$, ****$p < 0.0001$; one-way ANOVA for comparison in individual control and wheel groups, and nested t-test for comparing two groups).
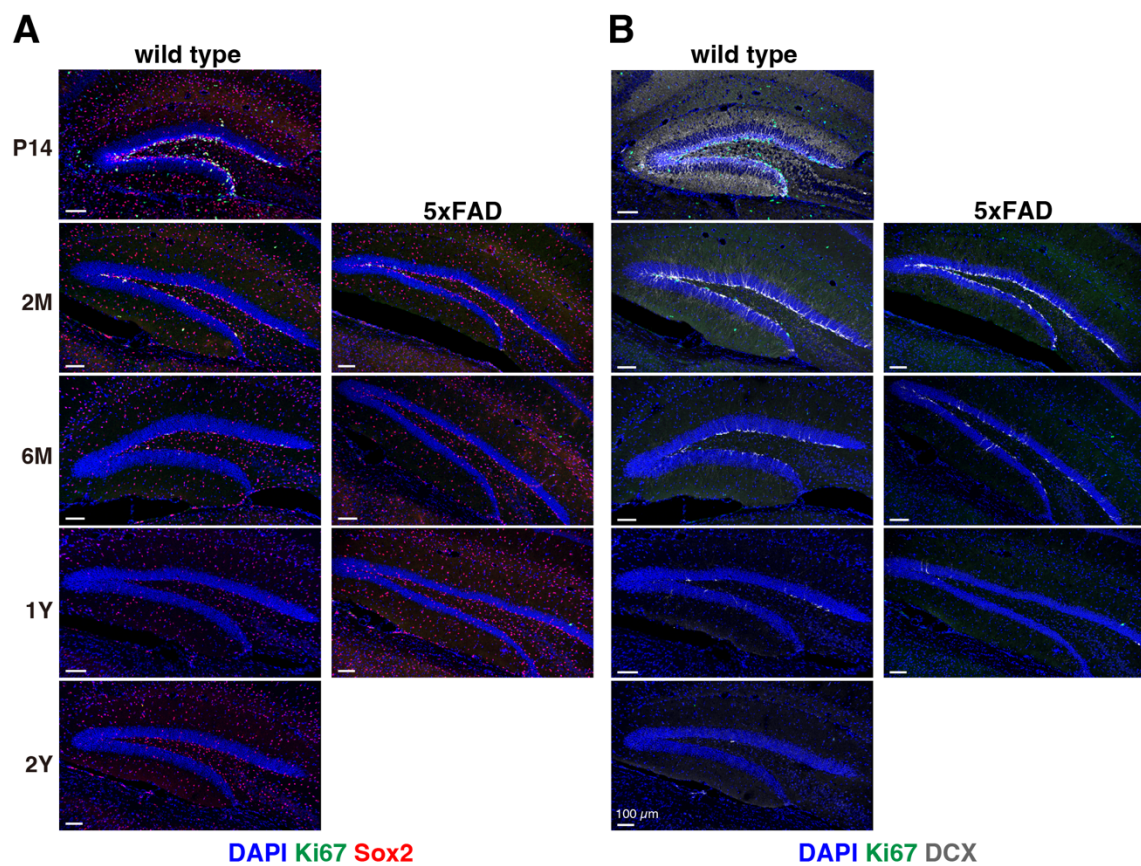
Fig. S4. Immunohistochemistry for counting proliferating NSCs and newly born neurons in LyMo wild-type and 5xFAD mice of different ages. Representative photos for counting proliferating Ki-67+ (green)/Sox2+ (red) cells **(A)** and Ki-67+ (green)/DCX+ (grey) cells **(B)** with DAPI (blue) in LyMo wild-type and 5xFAD mice of different ages. Scale bars, 100 μm.
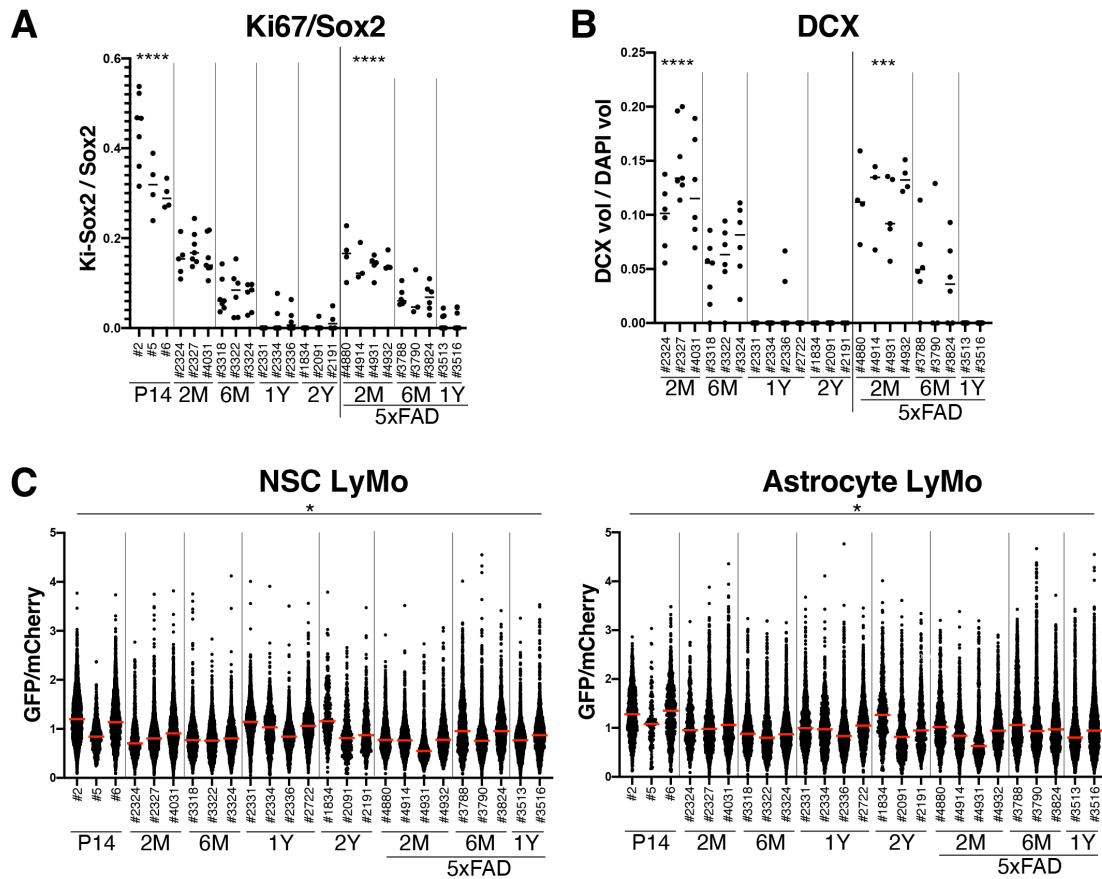
Fig. S5. NSC proliferation, neurogenesis, and lysosomal activity in individual mice of wild-type and 5xFAD mice of different ages. A, B. Number of proliferating NSCs (A; the ratio of Ki-67+/Sox2+ cells to Sox2+ cells) and newly born neurons (B; the ratio of Ki- 67+/DCX to DCX+ cells) in individual mice of LyMo wild-type and 5xFAD mice of different ages. # means the IDs of individual mice. C. LyMo measurement in individual mice. Result of LyMo measurement (GFP and mCherry ratio in mCherry spots) in NSCs (left) and astrocytes (right) of individual mice. Outliers with a value greater than ten of the GFP/mCherry ratio were excluded from statistical analyses. These figures correspond to Fig. 4A, B, D, and F. Red bars represent medians. (***$p < 0.001$, ****$p < 0.0001$; nested one-way ANOVA in the different age of wild-type and 5xFAD mice).
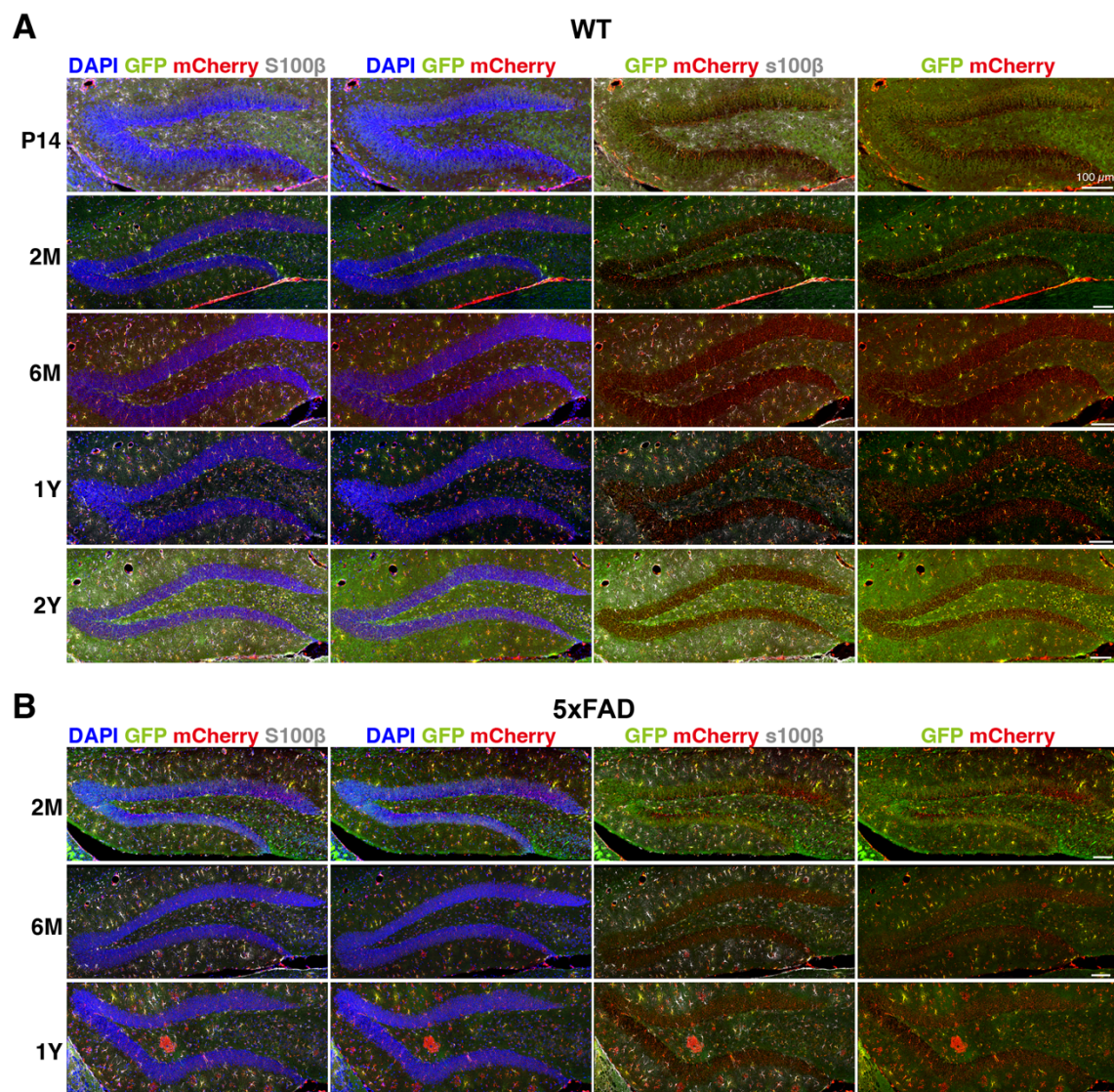
Fig. S6. Immunohistochemistry of LyMo wild-type and 5xFAD mice of different ages. Representative images for LyMo measurement of different age mice (A) (WT: wild type) and Alzheimer's disease model mice (B) (5xFAD) immunostained with GFP (green), mCherry (red) and S100β antibodies with DAPI (blue) with several combinations of separated colors. Scale bars, 100 μm.
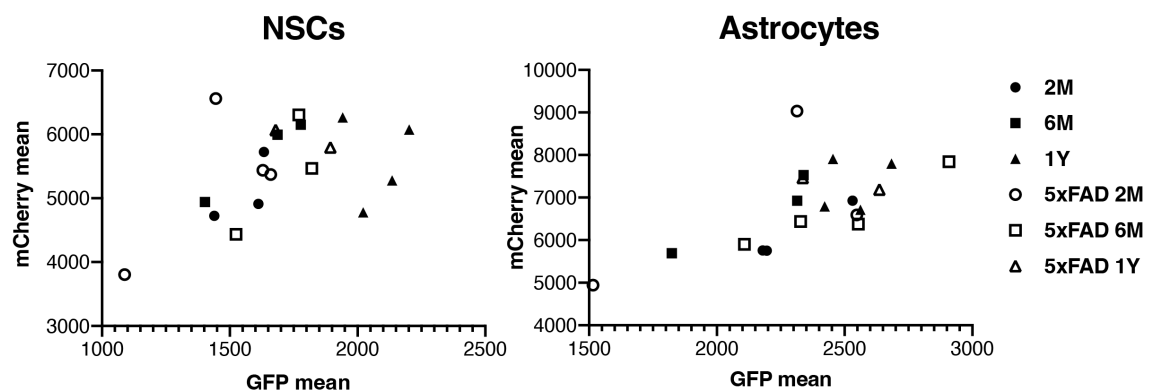
Fig. S7. LyMo expression levels in wild-type and 5xFAD mice. 2D plots indicate mean intensity values of GFP and mCherry in NSCs (left panel) and astrocytes (right panel) of individual mice. Intensities were obtained from IHC images of LyMo mice at different ages of two months (circle), six months (square), and one year (triangle) in wild-type (closed) and 5xFAD (open) mice. The intensities of LyMo mCherry differed between individual mice, but there was no correlation with age and genotype.